Chaos
An Interdisciplinary Journal of Nonlinear Science

RESEARCH ARTICLE | JANUARY 03 2025

Asymptotic convergence for the dynamics of a Duffing-like oscillator under scaling analyses

Special Collection: From Sand to Shrimps: In Honor of Professor Jason A. C. Gallas

André Luís Prando Livorati ; André Paganotti Faber; Daniel Borin

Chaos 35, 013108 (2025)
https://doi.org/10.1063/5.0233700

Asymptotic convergence for the dynamics of a Duffing-like oscillator under scaling analyses

Cite as: Chaos 35, 013108 (2025); doi: 10.1063/5.0233700
Submitted: 16 August 2024 · Accepted: 6 December 2024 ·
Published Online: 3 January 2025

André Luís Prando Livorati,[a] André Paganotti Faber, and Daniel Borin

AFFILIATIONS

IGCE—Physics Department, São Paulo State University (UNESP), 13506-900 Rio Claro, SP, Brazil

Note: This paper is part of the Focus Issue, From Sand to Shrimps: In Honor of Professor Jason A. C. Gallas.
[a]**Author to whom correspondence should be addressed:** andre.livorati@unesp.br

ABSTRACT

The dynamics of the convergence for the stationary state considering a Duffing-like equation are investigated. The driven potential for these dynamics is supplied by a damped forced oscillator that has a piecewise linear function. Fixed points and their basins of attraction were identified and measured. We used entropy basin techniques to characterize the basins of attraction, where a changeover in its boundary basin entropy is observed concerning the boundary length. Additionally, we have a set of polar coordinates to describe the asymptotic convergence of the dynamics based on the range of the control parameter and initial conditions. The entire convergence to the stationary state was characterized by scaling laws.

A Duffing-like equation is studied considering a driven potential given by a piecewise linear function. The modeling has applications in several areas, such as electronic circuits, synchronization, mechanical systems, and biology, among others. For a specific range of the control parameter, we set two attracting fixed points and characterized their basins of attraction. Through the analysis of the entropy basin, we observed a transition in the boundary basin entropy for a given critical control parameter. The results indicate a transition in the length of the basin boundary. To investigate the asymptotic convergence of the dynamics to the fixed points more precisely, we applied a linear to polar coordinates transformation, which presented itself as a useful metric for the description of the convergence to the stationary states, and by varying ranging the control parameter and initial conditions, an exponential decay to the fixed points was observed. We have proposed some scaling law arguments to describe this behavior, and the numerical results we obtained are in good agreement, since a single and universal plot was drawn. These results confirm the robustness of the formalism, which may be extended to other similar dynamical systems.

I. INTRODUCTION

Nonlinear differential equations are often used to describe the behavior of dynamical systems. Depending on the nonlinear terms involved in the equations, a rich variety of nonlinear phenomena can be observed, considering both conservative and dissipative dynamics.[1,2] A variation in the control parameters of the system may lead the dynamics to exhibit phase transitions, which, in the context of statistical mechanics, can be linked to abrupt changes in spatial structure.[3,4] In contrast, alterations in the phase space structure are specifically associated with phase transitions in dynamical systems.[5–7]

A useful technique to describe such phase transitions is scaling analysis, where near the criticality, the dynamics can be characterized via critical exponents,[8–14] especially if there is an asymptotic behavior of some physical observable.[15–20] In addition, scaling laws can contribute to the development of more precise and robust mathematical models for the description of complex phenomena.[21] The importance of scaling laws extends to several areas, including the physics of critical phenomena;[22] materials science;[23] macro, micro, and nanoscales;[24] multifractal objects;[25] astronomy;[26] fractional dynamics;[27] plasma physics;[28,29] biology;[30,31] and engineering;[32,33] among many other applications.[34]

One of the most widely researched nonlinear dynamical systems is the Duffing oscillator.[35] The nonlinear terms in the differential equation of this system make it possible to analyze several complex phenomena such as bifurcations,[36–38] resonance,[39–41] and chaotic transitions.[42–44] In addition, the nonlinear dynamics of the Duffing equation has direct applications in several areas, including biology,[45,46] laser dynamics,[47] materials engineering,[48–51] and electrical circuits,[52–55] among others.

In this paper, we revisit and investigate the dynamics of the convergence to a stationary state, for a set of differential equations given by a Duffing-like equation, where a damped forced oscillator, with a piecewise linear function sets the driven potential for the dynamics. In this scenario, fixed points are obtained and characterized, as well as their basins of attraction. We used entropy basins techniques[56–61] to characterize the basins and setup a changeover in the measure of the entropy basin for a critical parameter. The results indicate that there is a transition in the length of the basin boundary. Additionally, based on the range of the control parameter, we setup polar coordinates to describe dynamics, which seems to be a useful metric for investigating the behavior of convergence to the stationary state. Scaling laws were used to characterize the entire convergence to the stationary state, where a universal plot describes a scaling invariance through the initial conditions as well as the control parameter, giving robustness to our description of the dynamical scenario.

The paper is organized as follows: In Sec. II, we describe the model, chaotic properties, and the stability criteria for the fixed points. Section III is devoted to the numerical results considering investigations of basin entropy, asymptotic convergence to the fixed points, and scaling laws analysis. Finally, in Sec. IV, we present some final remarks and conclusions.

II. THE MODEL AND ITS PROPERTIES

Duffing's equation can describe the dynamics of some electrical and mechanical systems.[62] When considering a damped forced oscillator with mass m and displacement u, assuming the restitution force as non-linear and cubic described by $K(u) = k_0 u + k_1 u^3$, where k_0 and k_1 are the spring constants, and the viscous and linear damping is described by $C(u) = c\dot{u}$, where c is the damping, the following equation of motion is obtained:

$$m\ddot{u} + C(u) + K(u) = G(t), \tag{1}$$

where $G(t)$ is a periodic forcing force.

In this paper, we considered a Duffing-like equation to describe the dynamics of a damped oscillator, where all the variables are already setup as dimensionless. The displacement is now represented as x and the equation of motion is given by

$$\ddot{x} + b\dot{x} - F(x) = f(t), \tag{2}$$

the damping is given by $b\dot{x}$, the external periodic perturbation force is given by $f(t) = \varepsilon \sin(\omega t)$, with amplitude ε and frequency of oscillation ω. The term $F(x)$ is set as a piecewise linear function given by

$$F(x) = \begin{cases} -(x+1), & \text{if} \quad x < -1/2, \\ x, & \text{if} \quad -1/2 \le x \le 1/2, \\ -(x-1), & \text{if} \quad x > 1/2, \end{cases} \tag{3}$$

or rewriting in terms of absolute function

$$F(x) = -x + |x + 1/2| - |x - 1/2|. \tag{4}$$

The motivation for using the piecewise linear function, instead of the cubic potential term, lies in an application for electrical circuits.[52] Since in electronics it is difficult to setup nonlinear potential terms, an approximation by a piecewise linear function produces qualitatively very similar results in experimental analysis. Also, one can find applications of piecewise linear functions in vibrational signals,[63] stabilization of driven systems,[64] and chaotic attractors and bifurcations.[65]

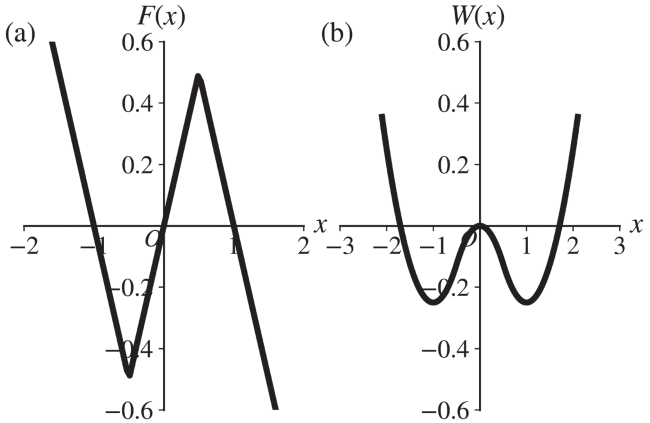

FIG. 1. Behavior of (a) the piecewise linear force $F(x)$, given by Eq. (3), and (b) the double well parabolic potential $W(x)$ given by Eq. (5).

The force given in Eq. (4) gives birth to a two-well parabolic potential as $W(x) = -\int F(x)dx$, where

$$W(x) = \begin{cases} x^2/2 + x + 1/4, & \text{if} \quad x < -1/2, \\ -x^2/2, & \text{if} \quad -1/2 \le x \le 1/2, \\ x^2/2 - x + 1/4. & \text{if} \quad x > 1/2. \end{cases} \tag{5}$$

Both behaviors of the functions $F(x)$ and $W(x)$ are displayed in Fig. 1.

Let us now set the equations used in this investigation. Considering the unperturbed version of Eq. (2), i.e., $\varepsilon = 0$, and the piecewise linear force, given in Eq. (4), we finally arrive at an equivalent set of two first order non autonomous equations, controlled by a single control parameter b,

$$\begin{cases} \dot{x} = y, \\ \dot{y} = -x + \left|x + \frac{1}{2}\right| - \left|x - \frac{1}{2}\right| - by. \end{cases} \tag{6}$$

The fixed points are obtained by setting $\dot{x} = \dot{y} = 0$, leading to $y = 0$ and $|x + 1/2| - |x - 1/2| - x = 0$. At the first absolute value of the previous equation, we can set $m_1 = |x + 1/2|$, and the second absolute value $m_2 = |x - 1/2|$. In the m_1 term, we have $(x + 1/2)$ if $x \ge -1/2$ and $(-x - 1/2)$ if $x < 1/2$, and in the m_2 term, we obtain $(x - 1/2)$ if $x \ge 1/2$ and $(-x + 1/2)$ if $x < 1/2$. After considering the intersection of both m_1 and m_2 absolute equations and the proper limits according to the functions $F(x)$ and $W(x)$ in Eqs. (3) and (5), it will lead us to three fixed points, $P_1^* = (x_1^*, y_1^*) = (0, 0)$, $P_2^* = (x_2^*, y_2^*) = (-1, 0)$, and $P_3^* = (x_3^*, y_3^*) = (1, 0)$.

Their stability is given by $\mathrm{Det}(J - \lambda I)|_{(x^*, y^*)} = 0$, where I denotes the identity matrix and λ are the eigenvalues of the Jacobin matrix J given by

$$J = \begin{pmatrix} 0 & 1 \\ F(x^*) & -b \end{pmatrix}, \tag{7}$$

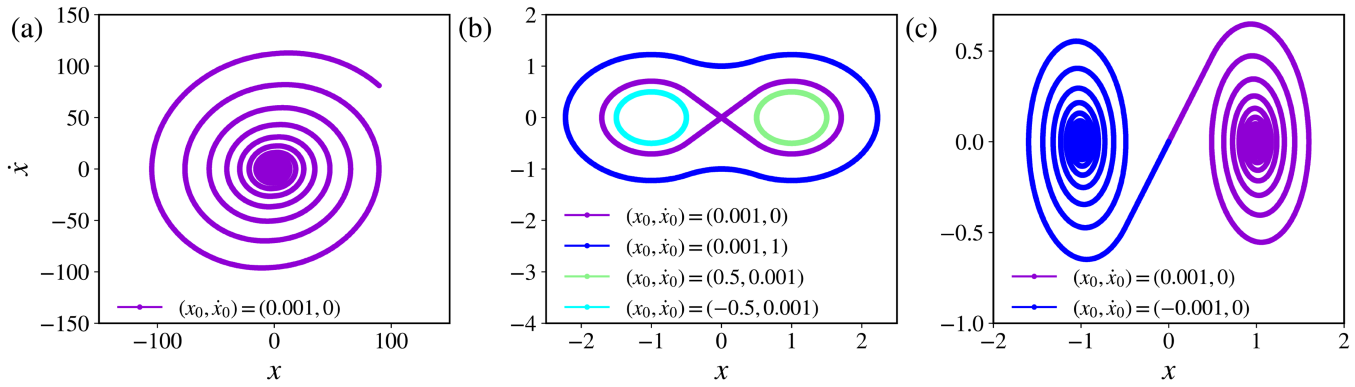

FIG. 2. Phase space of the dynamics for some values of the control parameter b. In (a), we have $b = -0.1$, indicating an unstable (source) orbit, in (b) we have $b = 0$, where a typical rotation, libration, and separatrix of orbits appears, and finally in (c) we have $b = 0.1$, where the orbits are asymptotically stable and converge to the fixed points P_2^* and P_3^*.

where

$$F(x^*) = -1 + \frac{x^* + \frac{1}{2}}{\left|x^* + \frac{1}{2}\right|} - \frac{x^* - \frac{1}{2}}{\left|x^* - \frac{1}{2}\right|} = \begin{cases} -1, & \text{if } |x^*| > 1/2, \\ 1, & \text{if } |x^*| < 1/2. \end{cases} \quad (8)$$

After a straightforward algebra, one may find the eigenvalues of Eq. (6) as

$$\lambda_{1;2} = \frac{1}{2}\left(-b \pm \sqrt{b^2 + 4F(x^*)}\right). \quad (9)$$

Analyzing these values allows us to classify the fixed point x^* based on the value of the control parameter b. When $|x^*| > 1/2$, it is a hyperbolic saddle point, regardless of the value of parameter b. However, for $|x^*| < 1/2$, the classification varies with the values of the parameter b. For instance, in $b = 0$ and $b = 2$ ($b = -2$), it becomes a center and a stable (unstable) improper node, respectively; for $0 < b < 2$ ($-2 < b < 0$), it transforms into a stable (unstable) spiral point; and for $b > 2$ ($b < -2$), it evolves into a stable (unstable) node.

One may find some of the behavior of the dynamics according to the fixed point stability in Fig. 2. In Fig. 2(a), we have $b = -0.1$, the fixed point is classified as a source and the orbit is unstable, so as the time evolves it gets apart from the fixed point. Concerning Fig. 2(b), we have $b = 0$, so the fixed points P_2^* and P_3^* are set as elliptic points and the fixed point P_1^* is a saddle. One can see that we have typical rotation and libration orbits, separated by a separatrix curve. Finally, in Fig. 2(c), we display the behavior for $b = 0.01$, where the orbits for both P_2^* and P_3^* fixed points are asymptotically stable. The range of interest for the control parameter b, which we focus on in this paper, is $0 < b < 1$, which includes this orbit behavior.

III. NUMERICAL RESULTS

In this section, we present some numerical results regarding the basins of attraction considering analysis through entropy basin techniques. We also show the asymptotic convergence for the fixed points, as well as the scaling arguments used to describe the dynamics as a function of the initial conditions and the control parameter.

A. Basins of attraction and basins entropy

Since we already know the dynamical scenario for the unperturbed Duffing-like oscillator as a function of the control parameter b, let us now focus on the range of interest, which includes the asymptotic convergence of the orbits, which is $0 < b < 1$. Figure 3 displays the basin of convergence for both fixed points $P_2^* = (-1, 0)$ and $P_3^* = (+1, 0)$. In Figs. 3(a)–3(c), the color black represents the basin of attraction for P_2^*, while orange (gray) denotes the basin of attraction for P_3^*. Each basin of Fig. 3 was constructed considering a grid of 1000×1000 initial conditions displayed in the x and $\dot{x}$ axes between the limits $[-5, +5]$ in both axes. The initial conditions were iterated in time up to 10^5, considering a integration step $h = 0.001$, in the fourth order Runge–Kutta numerical integrator.

One can see that as the control parameter b diminishes the frontiers of the basins are getting more and more embedded among each other. To characterize this behavior, we use a quantitative measure called basin entropy,[56–61] which captures the degree of uncertainty of a basin due to the fractality of the basin boundary. To evaluate it, we basically consider the following technique: a dynamical system with a bounded phase space region Ω that contains N_A attractors. We set Ω into a mesh of $N_B \times N_B$ blocks of linear size δ, where $N_B^2 \in \mathbb{N}$ denotes the total number of blocks. Each block contains a large number $N_s \times N_s$ of initial conditions where $N_s \in \mathbb{N}$, each leading to one of the N_A attractors. For each block i, we associate a probability p_{ij} of the attractor j to exist in this block and define the Gibbs entropy of the ith block as

$$S_i = -\sum_{j=1}^{n_i} p_{ij} \log_2 p_{ij}, \quad (10)$$

where $n_i \in [1, N_A]$ is the number of different attractors inside the ith block. The probability p_{ij} is the ratio of the number of initial conditions with attractor j to the total number of initial conditions in the block. In this paper, we consider a grid of $N_G \times N_G = 1000 \times 1000 = 10^6$ initial conditions (in similar way to Fig. 3) and perform the entropy calculation on blocks, which contains $N_s \times N_s = 10 \times 10 = 100$ initial conditions. Thus, considering that the

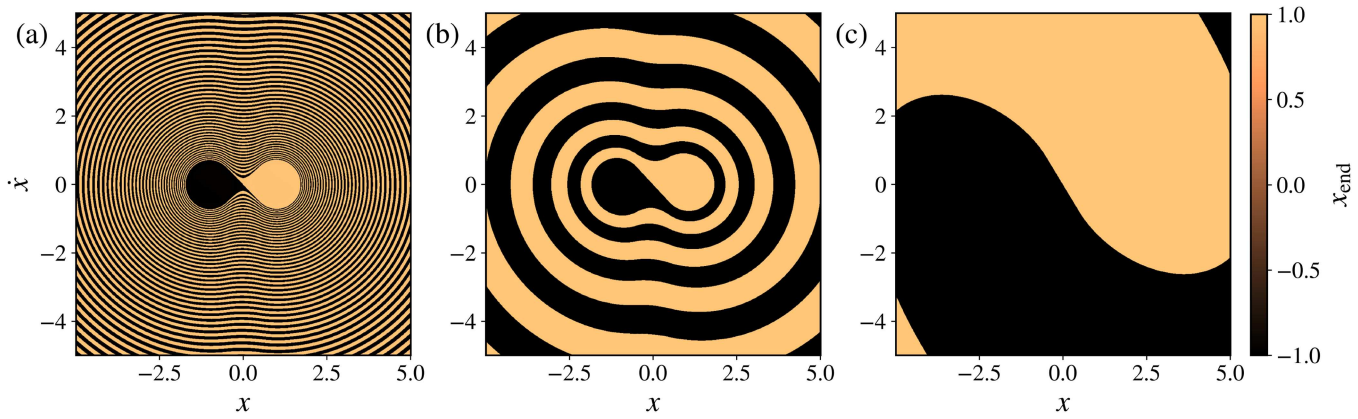

FIG. 3. The basins of attraction for the system of Eq. (6) considering (a) $b = 0.01$, (b) $b = 0.1$, and (c) $b = 1$. The color black represents the attracting basin for P_2^*, and the color orange (gray) displays the basin for P_3^*. One can see that when the value of the control parameter b gets smaller, the basins are getting embedded with thinner and thinner layers. Multimedia available online.

blocks are non-overlapping, the entropy of Ω is basically the sum of the entropy of all blocks, as described below:

$$S = \sum_{i=1}^{N_G^2} S_i. \tag{11}$$

In order to describe the basin boundaries of the attractors, we use the basin boundary entropy S_{bb}, defined as

$$S_{bb} = \frac{S}{N_C}, \tag{12}$$

where N_C is the number of boxes that contains more than one attractor. This observable measures the uncertainty related to the basin boundary, following the fractality criterion.[56] According to this criterion, if $S_{bb} > \log_2 2 = 1$, the boundary is considered fractal. However, it is important to note that even if the boundary is fractal, S_{bb} might not always satisfy this condition.

Figure 4 illustrates the behavior of S_{bb} as b varies for several values of N_s. Note that for small values of the control parameter b, the boundary basin entropy S_{bb} is greater than 1. However when b is around 0.06, S_{bb} exhibits a changeover, dropping below 1. This behavior does not change even when we vary the number of boxes considered to compute the boundary basin entropy.

To explain this, our best guess lies in the system itself. Since the system under investigation is two-dimensional, it inherently prevents the presence of the unstable chaotic sets responsible for fractal basin boundaries.[66] This suggests that the system cannot exhibit fractal basin boundaries. Instead, the transition seems to occur in the length of the basin boundary itself. For $b = 0.01$, the boundary is significantly longer and embedded than for $b = 0.1$ and $b = 1.0$, as illustrated in Fig. 3. We believe that the boundary basin entropy is detecting this change in boundary length rather than a transition to fractal behavior. In addition, the relation between each value of S_{bb} and its corresponding attraction basins is illustrated in a video attached in the multimedia files, where $N_s = 10$.

B. Asymptotic convergence and scaling analysis

The behavior of the basins of attraction and the changeover in the S_{bb}displayed in Sec. III A generates an issue in our dynamical description, i.e., if we have a small enough control parameter b, it would be basically impossible to set, with a given precision, a proper initial condition that converges to P_2^* or P_3^*.

To avoid this issue, we have set a re-scale in the system's variables. Instead of using linear coordinates, as shown in Eq. (6), we utilized a transformation to polar coordinates, as $(x, y) \to (r, \phi)$, given by

$$\begin{cases} r(t) = \sqrt{(x(t))^2 + (\dot{x}(t))^2}, \\ \phi(t) = \tan^{-1}\left(\dot{x}(t)/x(t)\right), \end{cases} . \tag{13}$$

where $r(t)$ is the distance from the origin to the orbit at a given time t and $\phi(t)$ is the angle concerning the horizontal positive semi-axis. With this change in the variables, the new fixed points become $P^*(r^*, \phi^*) = (1, 0)$. Such change in the variables sets a new scenario for dynamics description.

The radial distance $r(t)$ becomes a useful metric for investigating the behavior of convergence to the stationary state. Figure 5(a) displays how the radial position $r(t)$ is given, basically considering the Euclidean distance from the orbit to the origin. Indeed, in Fig. 5(b), it is possible to see the convergence for some values of initial ratio r_0 and for different values of the control parameter b. All the decay curves exhibit similar behavior, initially characterized by an exponential decay followed by a steady plateau at $r(t) = 1$ after a significant transient. The exponential function that describes the decay is given by

$$r(t) = A \exp(-\xi t), \tag{14}$$

where A is the constant of the exponential fit and ξ is the exponent that indicates how fast the decay rate evolves.

One can see in Fig. 5(b) that the control parameter b influences the crossover time of the decay rate of the orbits, i.e., for smaller values of b the decay rate starts in long times, and it starts earlier for

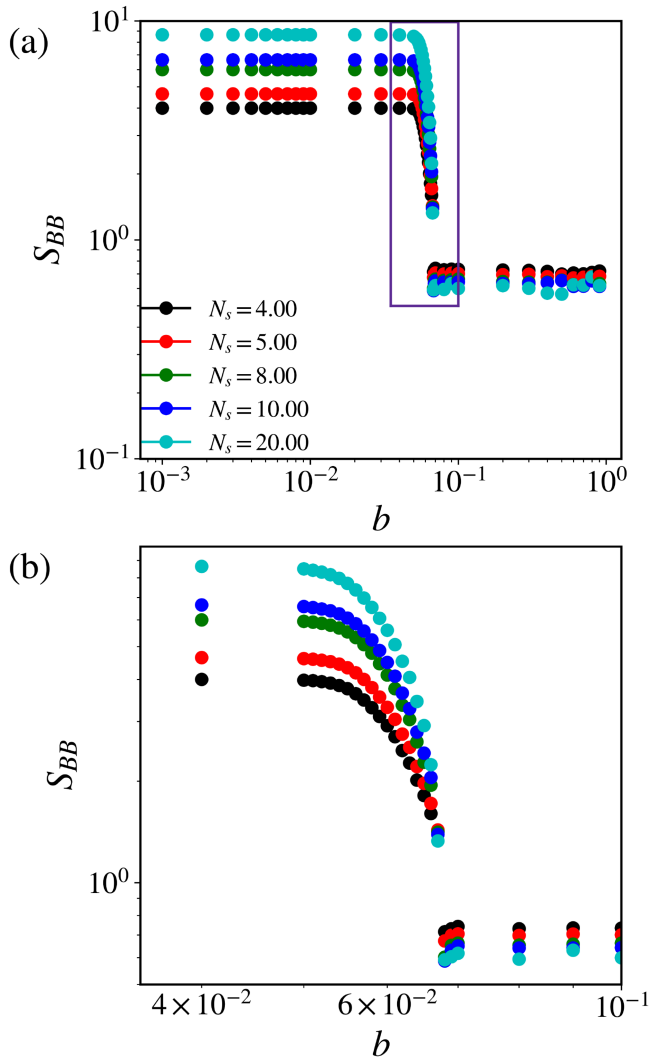

FIG. 4. In (a), we have the basin entropy S_b for different ranges of N_s, indicating a changeover in its behavior according to the parameter b evolves and in (b) we display a zoom-in window of the region depicted in (a) for the range of $b \in [0.035, 0.1]$ and $S_{BB} \in [0.5, 9.9]$, indicating that there is a critical parameter near around $b_c \approx 0.06$. Multimedia available online.

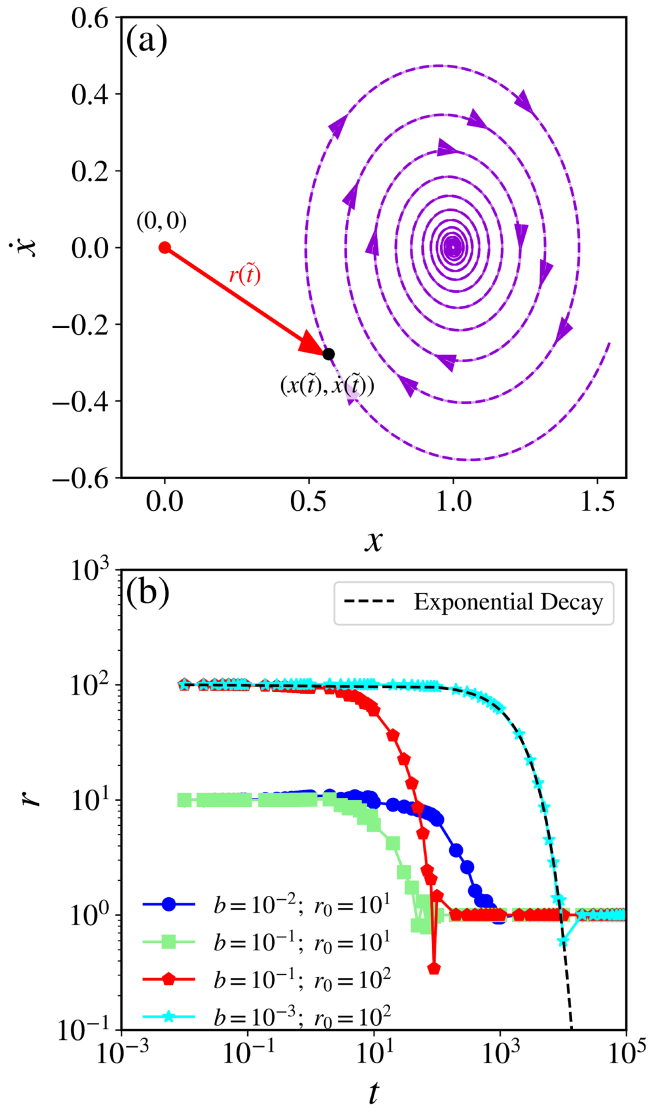

FIG. 5. In (a), we display how the variable $r(t)$ is set as the distance from the origin to the orbit, until it converges to the rearranged fixed point $P^*(r^*, \phi^*) = (1, 0)$. In (b), we have the behavior of the $r(t)$ curves as a function of time for different initial conditions r_0 and some values of the control parameter b. The curves exhibit an exponential decay until they reach a convergent plateau at $r = 1$ indicating the convergence to the fixed point.

higher values of b. On the other hand, the value of the initial condition r_0 does not influence the decay rate. It only deals with the initial vertical orbits of plateaus. The similarity of these curves suggests that the convergence is scaling invariant with respect to the control parameter b and the initial conditions r_0.

In order to investigate the scaling invariance possibility, we extend the range of the control parameter $b \in [0.001, 1.0]$ and considered several different initial conditions $r_0 \in [10^2, 10^4]$ and evolved the dynamics of $r(t)$ for long times (up until $t = 10^5$), again considering a integration step $h = 0.001$, in the fourth order Runge–Kutta numerical integrator, as mentioned before. In Fig. 6(a), one can see the behavior of the $r(t)$ curves. The initial conditions r_0 are responsible for the initial plateaus, and the control parameter b controls the crossover time when the orbits start to decay.

After considering an exponential fit, according to Eq. (14) in the decay rate of all the $r(t)$ curves, we investigate the dependence of the exponent ξ on the control parameters. Since the initial conditions r_0 do not affect the crossover time, they only lead to significant

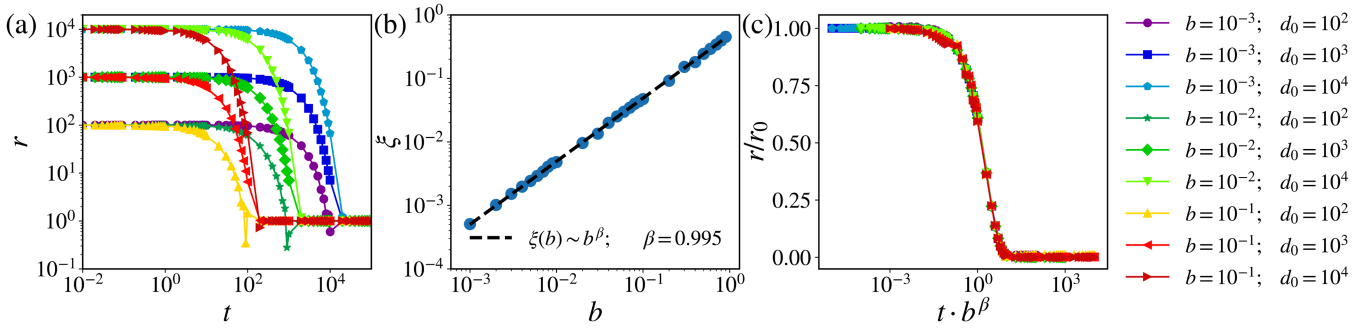

FIG. 6. In (a), we show the radial distance $r(t)$ as a function of time t for different values of b and r_0. The decay rates of these curves are described by $r \approx \exp(-\xi)$, where ξ is the decay exponent. In (b), for fixed $r_0 = 10^{-2}$, a very good power law fitting shows that the relation between ξ and b is given by $\xi(b) \sim b^{\beta}$, with $\beta = 0.995$. Finally in (c), after a proper re-arrangement of the axes as $t \to t \cdot b^{\beta}$ and $r \to r/r_0$, all the data overlap into a single and universal plot, thereby characterizing and confirming our scaling arguments.

changes in the constant A. On the other hand, the behavior of the control parameter b influences the behavior of ξ. Figure 6(b) shows a power law fit concerning the range of the control parameter b and the value of the exponent ξ for a constant value of the initial condition $r_0 = 10^2$. The numerical adjustment furnishes us with the following equation:

$$\xi(b) = Cb^{\beta}, \tag{15}$$

where C is the constant of the power law fit and $\beta = 0.995 \approx 1.0$ is the critical exponent.

Taking Eq. (15) into account along with the value of the exponent β, we can rearrange the axes of Fig. 6(a) to validate the proposed scaling arguments. By dividing the vertical axis $r(t)$ by the value of the initial conditions r_0, we normalize all the initial plateaus to the unity. Considering the time axis, we multiply each one of the curves by b^{β}. One can see in Fig. 6(c) the transformations mentioned above applied to the axis and in the $r(t)$ curves of Fig. 6(a). Such transformations give birth to a perfect collapse of all the decay rate curves of $r(t)$ into a single and universal plot. This behavior confirms the validity of our scaling arguments, including the change in the variables of the system, from linear to polar ones, which sets a useful metric for investigating the behavior of convergence to the stationary state, also gives robustness to our results and numerical analysis.

IV. FINAL REMARKS

In summary, we have considered a damped forced oscillator with a linear by parts function that creates a driven potential for the dynamics. We analyzed the dynamics of the convergence for stationary state for a set of differential equations generated by a Duffing-like equation. Fixed points and their associated basins of attraction were obtained and described. We used the entropy basins technique to set and characterize the basins of attraction, according to the range of the control parameter. The results reveal a changeover in the basin of attraction near a critical parameter b_c, indicating that there is a transition in the length of the basin boundary. However, the characterization of this changeover as a phase transition itself still needs further investigation.

To characterize the asymptotic convergence of the dynamics, we employed polar coordinates according to the range of the control parameter. Scaling laws were obtained to characterize the asymptotic convergence to the stationary state. A universal plot, describing the decay curves considering a variation in the initial conditions and the control parameter, was obtained. These results lead robustness to our representation of the dynamical scenario, including the transformation of the variables of the systems, from linear to polar coordinates, which was setup as a new investigation scenario for the convergence of the stationary state and also validate the scaling analysis.

As a perspective, we intend to study the perturbation version of the Duffing-like equation in order to analyze the stable and unstable manifold scenarios for the basins of attraction, and check if there is any influence on the transition of the boundary basin entropy.

ACKNOWLEDGMENTS

A.L.P.L. acknowledges Brazilian agencies FAPESP, CNPq, and CAPES for financial support. D.B. acknowledges the financial support of the São Paulo Research Foundation (FAPESP), under Grant Nos. 2022/03612-6 and 2024/06749-8.

AUTHOR DECLARATIONS

Conflict of Interest

The authors have no conflicts to disclose.

Author Contributions

André Luís Prando Livorati: Conceptualization (equal); Data curation (equal); Formal analysis (equal); Funding acquisition (equal); Investigation (equal); Methodology (equal); Project administration (equal); Resources (equal); Software (equal); Supervision (equal); Validation (equal); Visualization (equal); Writing – original draft (equal); Writing – review & editing (equal). **André Paganotti Faber:** Data curation (equal); Formal analysis (equal); Investigation (equal); Methodology (equal); Resources (equal); Software (equal); Validation (equal); Writing – original draft (equal); Writing – review &

editing (equal). **Daniel Borin:** Data curation (equal); Formal analysis (equal); Investigation (equal); Methodology (equal); Resources (equal); Software (equal); Validation (equal); Writing – original draft (equal); Writing – review & editing (equal).

DATA AVAILABILITY

The data that support the findings of this study are available from the corresponding author upon reasonable request.

REFERENCES

[1]A. J. Lichtenberg and M. A. Lieberman, "Regular and chaotic dynamics," in *Applied Mathematical Sciences* (Springer Verlag, New York, 1992), Vol. 38.
[2]R. C. Hilborn, *Chaos and Nonlinear Dynamics: An Introduction for Scientists and Engineers* (Oxford University Press, New York, 1994).
[3]K. T. Alligood, T. D. Sauer, and J. A. Yorke, *Chaos: An Introduction to Dynamical Systems* (Springer Verlag, New York, 1996).
[4]P. Gaspard, *Chaos, Scattering and Statistical Mechanics* (Cambridge University Press, Cambridge, 1998).
[5]R. K. Pathria, *Statistical Mechanics* (Elsevier, Burlington, 2008).
[6]G. M. Zaslasvsky, *Physics of Chaos in Hamiltonian Systens* (Imperial College Press, New York, 2007).
[7]A.-L. Barabási and H. E. Stanley, *Fractal Concepts in Surface Growth* (Cambridge University Press, Cambridge, 1985).
[8]E. D. Leonel, P. V. E. McClintock, and J. K. L. da Silva, Phys. Rev. Lett. **93**, 014101 (2004).
[9]E. D. Leonel, Phys. Rev. Lett. **98**, 114102 (2007).
[10]A. L. P. Livorati, D. G. Ladeira, and E. D. Leonel, Phys. Rev. E **78**, 056205 (2008).
[11]J. A. de Oliveira, R. A. Bizão, and E. D. Leonel, Phys. Rev. E **81**, 046212 (2010).
[12]D. F. M. Oliveira, J. Vollmer, and E. D. Leonel, Physica D **240**, 389 (2011).
[13]D. F. M. Oliveira, M. Robnik, and E. D. Leonel, Phys. Lett. A **376**, 723 (2012).
[14]D. R. da Costa, A. L. P. Livorati, and E. D. Leonel, Int. J. Bifurcation Chaos **22**, 250250 (2012).
[15]C. M. Kuwana, J. A. de Oliveira, and E. D. Leonel, Physica A **395**, 458 (2014).
[16]R. M. N. Teixeira *et al.*, Phys. Lett. A **379**, 1246 (2015).
[17]E. D. Leonel *et al.*, Phys. Lett. A **379**, 1808 (2015).
[18]J. A. Méndez-Bermúdez, J. A. de Oliveira, R. Aguilar-Sánchez, and E. D. Leonel, Physica A **436**, 943 (2015).
[19]J. A. Méndez-Bermúdez, A. J. Martínez-Mendoza, A. L. P. Livorati, and E. D. Leonel, J. Phys. A **48**, 405101 (2015).
[20]E. D. Leonel, Commun. Nonlinear Sci. Numer. Simul. **39**, 520 (2016).
[21]E. D. Leonel, *Scaling Laws in Dynamical Systems* (Springer, Singapore, 2021).
[22]B. I. Halperin and P. C. Hohenberg, Phys. Rev. **177**, 952 (1969).
[23]V. Franco and A. Conde, Int. J. Refrig. **33**, 465 (2010).
[24]M. Wautelet, Eur. J. Phys. **22**, 601 (2001).
[25]G. Paladin and A. Vulpiani, Phys. Rep. **156**, 147 (1987).
[26]B. J. T. Jones, V. J. Martínez, E. Saar, and V. Trimble, Rev. Mod. Phys. **76**, 1211 (2005).
[27]D. Borin, Chaos, Solitons Fractals **181**, 114597 (2024).
[28]D. D. Ryutov, Phys. Plasmas **25**, 100501 (2018).
[29]R. Marino and L. Sorriso-Valvo, Phys. Rep. **1006**, 1 (2023).
[30]G. B. West, J. H. Brown, and B. J. Enquist, Science **276**, 122 (1997).
[31]G. B. West, Physica A **263**, 104 (1999).
[32]Z. P. Bažant, J. Eng. Mech. **119**, 1828 (1993).
[33]G. I. Barenblatt, A. J. Chorin, and V. M. Prostokishin, Appl. Mech. Rev. **50**, 413 (1997).
[34]D. Borin, A. L. P. Livorati, and E. D. Leonel, Chaos, Solitons Fractals **175**, 113965 (2023).
[35]G. Duffing, *Erzwungene Schwingungen bei Veranderlicher Eigenfrequenz* (Friedrich Vieweg Und Sohn, Braunschweig, 1918) (in German).
[36]P. Holmes, Philos. Trans. R. Soc. London A **292**, 419 (1979).
[37]J. G. Freire, M. R. Gallas, and J. A. C. Gallas, Europhys. Lett. **118**, 38003 (2017).
[38]C. Bonatto, J. A. C. Gallas, and Y. Ueda, Phys. Rev. E **77**, 026217 (2008).
[39]A. Sack, J. G. Freire, E. Lindberg, T. Pöschel, and J. A. C. Gallas, Sci. Rep. **3**, 3350 (2013).
[40]A. Gusso, S. Ujevic, and R. L. Viana, Nonlinear Dyn. **103**, 1955 (2021).
[41]A. R. Zeni and J. A. C. Gallas, Physica D **89**, 71 (1995).
[42]R. C. Bonetti, C. A. S. Batista, A. M. Batista, S. E. de S. Pinto, S. R. Lopes, and R. L. Viana, Phys. Rev. E **78**, 037102 (2008).
[43]A. Izadbakhsh and N. Nikdel, Chaos, Solitons Fractals **153**, 111433 (2021).
[44]J. Song and X. Han, Chaos, Solitons Fractals **178**, 114350 (2024).
[45]R. Belousov, F. Berger, and A. J. Hudspeth, Phys. Rev. E **99**, 042204 (2019).
[46]F. Sadyrbaev and I. Samuilik, "Computational and Mathematical Models in Biology" in *Nonlinear Systems and Complexity* (Springer, 2023), Vol. 38, p. 159.
[47]J. A. C. Gallas, Atom. Phys. **51**, 919 (2021).
[48]G. Sebald *et al.*, Smart Mater. Struct. **20**, 102001 (2011).
[49]R. Masana and M. F. Daqaq, J. Sound Vib. **332**, 6755 (2013).
[50]L. F. Ziebell and J. A. C. Gallas, Eur. Phys. J. Plus **138**, 930 (2023).
[51]Y. Zhang, H. Mao, H. Mao, and Z. Huang, Results Phys. **7**, 3243 (2017).
[52]E. Tamaseviciute *et al.*, Nonlinear Anal.: Model. Control **13**(2), 241 (2008).
[53]F. Battelli and K. J. Palmer, J. Differ. Equ. **101**, 276 (1993).
[54]R. C. Bonetti *et al.*, J. Phys. A **47**, 405101 (2014).
[55]B. K. Jones and G. Trefan, Am. J. Phys. **69**, 464 (2001).
[56]A. Daza, A. Wagemakers, B. Georgeot, D. Guéry-Odelin, and M. A. F. Sanjuán, Sci. Rep. **6**, 31416 (2016).
[57]J. P. Tarigo, C. Stari, C. Masoller, and A. C. Martí, Chaos **34**, 053113 (2024).
[58]A. Wagemakers, A. Daza, and M. A. F. Sanjuán, Chaos, Solitons Fractals **175**, 113963 (2023).
[59]M. Mugnaine *et al.*, Europhys. Lett. **125**, 58003 (2019).
[60]M. Mugnaine *et al.*, Phys. Rev. E **97**, 012214 (2018).
[61]M. Mugnaine *et al.*, Chaos **31**, 023125 (2021).
[62]I. Kovacic and M. J. Brennan, *The Duffing Equation: Nonlinear Oscillators and Their Behaviour* (Wiley Publication, 2011).
[63]P. Jia, J. Yang, C. Wu, and M. A. F. Sanjuán, J. Vib. Control **25**, 141 (2019).
[64]B. Ahmad, J. Nonlinear Dyn. **2013**, 824701 (2013).
[65]S. V. Priyatharsini, B. Bhuvaneshwari, V. Chinnathambi, and S. Rajasekar, J. Sci. Res. **13**, 361 (2021).
[66]X. Chen, T. Nishikawa, and A. E. Motter, Phys. Rev. X **7**, 021040 (2017).